

THREE DISCRETE GROUPS WITH HOMOGENEOUS CHEMISTRY ALONG THE RED GIANT BRANCH IN THE GLOBULAR CLUSTER NGC 2808¹EUGENIO CARRETTA²

ABSTRACT

We present the homogeneous reanalysis of Mg and Al abundances from high resolution UVES/FLAMES spectra for 31 red giants in the globular cluster NGC 2808. We found a well defined Mg-Al anticorrelation reaching a regime of subsolar Mg abundance ratios, with a spread of about 1.4 dex in $[\text{Al}/\text{Fe}]$. The main result from the improved statistics of our sample is that the distribution of stars is not continuous along the anticorrelation as they are neatly clustered into three distinct clumps each with different chemical composition. One group (P) shows the primordial composition of field stars of similar metallicity, and the other two (I and E) have increasing abundances of Al and decreasing abundances of Mg. The fraction of stars we found in the three components (P: 68%, I: 19%, E: 13%) is in excellent agreement with the number ratios computed for the three distinct main sequences in NGC 2808: for the first time there is a clear correspondence between discrete photometric sequences of dwarfs and distinct groups of giants with homogeneous chemistry. The composition of the I group cannot be reproduced by mixing of matter with extreme processing in hot H-burning and gas with pristine, unprocessed composition, as also found in the recent analysis of three discrete groups in NGC 6752. This finding suggests that different classes of polluters were probably at work also in NGC 2808.

Subject headings: Globular clusters: general — Globular clusters: individual (NGC 2808) — Stars: abundances — Stars: evolution — Stars: Population II

1. INTRODUCTION

Since decades the evidence of multiple stellar populations in globular clusters (GCs) was hidden in plain sight in spectroscopic observations (Gratton et al. 2012). The large star-to-star abundance variations in light elements (depletion of C, O, Mg anticorrelated with enhancement of N, Na, and Al) were understood as the simultaneous action of the NeNa and MgAl cycles in the same regions where the ON part of the CNO cycle is fully operative in H-burning at high temperature (Denisenkov & Denisenkova 1989; Langer et al. 1993). The pivotal study by Gratton et al. (2001) changed forever our perspective. Their finding of Na-O and Al-Mg anticorrelations among unevolved stars in NGC 6752 was the clearcut proof that these objects were formed by gas polluted by ejecta of more massive stars of a past generation, since the currently observed stars cannot synthesize the involved elements. Thus, whenever such anticorrelations are traced, we are witnessing the presence of multiple stellar generations.

The most outstanding signature, the Na-O anticorrelation discovered by the Lick-Texas group (see Kraft 1994), has been the subject of our ongoing FLAMES survey of 24 GCs (Carretta et al. 2006, 2009a,b, 2010, 2014, and references therein). Well quantified by the interquartile range of the $[\text{O}/\text{Na}]$ ratio (Carretta 2006, hereinafter Paper I) the homogeneous study of this feature shows that the phenomenon of multiple populations is primarily driven by the cluster total mass (Carretta et al. 2010) and it is tightly linked to the

horizontal branch (HB) morphology (Carretta et al. 2007a; Gratton et al. 2010). However, the Na-O anticorrelation cannot provide useful enough information on the discrete or continuous nature of multiple populations due to the intrinsic difficulty in measuring oxygen abundances: often, only the broad division of stars in first and second generations with different composition is revealed (e.g. Marino et al. 2008; Carretta et al. 2009a; Johnson & Pilachowski 2012; Cordero et al. 2014; Carretta et al. 2014).

On the other hand, the increasing precision in photometric data detects split sequences at all evolutionary phases, mainly due to the work by Milone and collaborators (see Milone et al. 2008, 2012, 2013). In turn, discrete sequences mean interruptions in the injection of ejecta in the intracluster gas, and by calibrating the quiescent periods we may hope to provide more stringent constraints on the still elusive nature of the early generation polluters such as intermediate mass asymptotic giant branch (AGB) stars (Ventura et al. 2001) or fast rotating massive stars (FRMS; Decressin et al. 2007).

Very promising is the Mg-Al anticorrelation, only found in massive and/or metal-poor clusters (e.g. Carretta et al. 2009b; Yong et al. 2005). Recently Carretta et al. (2012) found that in NGC 6752 red giant branch (RGB) stars are clearly clustered around three distinct values of Al, with groups nicely corresponding to the three photometric sequences revealed by Strömgren photometry on the RGB (Carretta et al. 2011). It seems that the $[\text{Al}/\text{Mg}]$ ratio is very efficient in enhancing the signal of homogeneous subgroups, especially in GCs with $[\text{Fe}/\text{H}] \leq -1$. We then applied the same approach to the globular cluster NGC 2808.

NGC 2808 is the ideal target for exploring the connection between distinct photometric sequences and dis-

¹ Based on data collected at the ESO telescopes under programme 072.D-0507 and during the FLAMES Science Verification programme with the UVES spectrograph.

² INAF, Osservatorio Astronomico di Bologna, via Ranzani 1, 40127, Bologna, Italy. eugenio.carretta@oabo.inaf.it

crete populations with homogeneous chemistry. It is massive ($M_V = -9.39$ mag; Harris 1996), moderately metal-poor, with three distinct main-sequences (MS: Piotto et al. 2007; Milone et al. 2012) and a multimodal distribution of stars on the HB (see Bedin et al. 2000). This GC has been the target of extensive abundance analysis by our group. Carretta et al. (2004a) derived the Na-O anticorrelation in this cluster from 19 RGB stars, while other light elements (including Mg, Al, Si) were studied for the same sample in Paper I. Na, O abundances for 120 giants and Al, Mg abundances for another limited sample of 12 RGB stars were obtained in Carretta et al. (2006) and Carretta et al. (2009b), respectively. Finally, Gratton et al. (2011) analyzed high resolution spectra of 42 stars on the HB of NGC 2808.

However, a complete study of the Mg-Al pattern in NGC 2808 was hampered by the lack of large samples with homogeneous analysis, since the adopted scales of atmospheric parameters were different in Paper I and in Carretta et al. (2009b). In the present Letter we derive Mg and Al abundances for 31 red giants in NGC 2808. The high degree of homogeneity of the analysis coupled with small internal errors highlight that stars are clustered around three distinct levels of Al and Mg. The number ratios of these subgroups are found to be in excellent correspondence with the number of stars in the three MSs.

2. DATA AND ANALYSIS

Here we present the abundances of Al and Mg for all the 31 stars observed with FLAMES/UVES. The UVES Red Arm fed by FLAMES fibers provides a wavelength coverage from 4800 to 6800 Å with a resolution of $R \simeq 45,000$, hence abundances of Al can be derived from the subordinate doublet at 6696-98 Å (not available in the GIRAFFE setups used for the Na-O anticorrelation). The whole sample include 19 stars from the FLAMES Science Verification (hereinafter sample SV, see Paper I) and 12 giants from the FLAMES survey (sample NAO, Carretta et al. 2006, 2009b, ESO Programme 072.D-0507), spanning the three brightest magnitudes along the RGB of NGC 2808 (see Fig. 1). Details of the observations and data reduction can be found in the original papers.

The novelty of the present analysis is the use for the entire sample of our well tested procedure for the derivation of atmospheric parameters, in particular the effective temperature T_{eff} . First pass values are from $V - K$ colors and the calibrations of Alonso et al. (1999, 2001). These were the temperatures actually adopted in Paper I (sample SV). The final T_{eff} values for all targets were however obtained using an average relation between the temperatures derived in this first step and the apparent magnitude of stars. This procedure was successfully used in our survey of 24 GCs to decrease the star-to-star errors in abundances due to uncertainties in temperatures, since magnitudes of bright RGB stars can be measured with higher precision than colors.

For NGC 2808, affected by relatively high differential (Bedin et al. 2000) reddening ($(E(B-V)=0.22$ mag, Harris 1996) the relation was derived as a function of the K magnitudes from 2MASS (Skrutskie et al. 2006), minimizing the impact of the differential reddening in the derived T_{eff} . Optical V magnitudes are from

Bedin et al. (2000). For the 12 giants of the NAO sample the new temperatures differ on average by about 5 K from the previous values. The new temperatures are on average higher by 27 K, although with a large scatter (118 K), for the SV sample.

Surface gravities were obtained from the position in the color-magnitude diagram (CMD), using the derived T_{eff} s, the distance modulus $(m - M)_V = 15.59$ mag from Harris (1996), bolometric corrections from Alonso et al. (1999), a mass of $0.85 M_{\odot}$ for all stars and $M_{\text{bol},\odot} = 4.75$ for the Sun, as in our previous studies of other 23 GCs. Values of the microturbulent velocity v_t were obtained by eliminating trends in the relation between abundances from Fe I lines and expected line strength (Magain 1984).

Equivalent widths (EW s) of the two Al lines and of two to three high excitation Mg lines (5711, 6318, and 6319 Å) were measured with the ROSA package (Gratton 1988). The abundances were derived using the atmospheric parameters determined for each star, interpolating within the Kurucz (1993) solar-scaled grid, with the overshooting option switched off. The adopted line lists and atomic parameters are from Gratton et al. (2003).

Derived LTE abundances of Mg and Al are listed in Table 1 together with optical B, V , and K magnitudes. For completeness, we also list the atmospheric parameters derived in the full abundance analysis (Carretta et al., in preparation). Adopted solar reference abundances are 7.43 dex for Mg and 6.23 dex for Al (Gratton et al. 2003; Carretta et al. 2004b).

Typical star-to-star errors in abundance ratios are 0.058 and 0.047 dex for $[Al/Fe]$ and $[Mg/Fe]$, respectively, due to internal errors in the adopted atmospheric parameters (5 K in T_{eff} , 0.04 dex in $\log g$, 0.03 dex in $[Fe/H]$, 0.05 kms^{-1} in v_t) and EW measurements; all errors were estimated as described in details in Carretta et al. (2007b, 2009b).

3. THREE DISTINCT GROUPS ON THE RGB IN NGC 2808

The $[Mg/Fe]$ and $[Al/Fe]$ abundance ratios (and their sum) are plotted as a function of the temperature in Fig. 2 (upper panel). No trend as a function of T_{eff} (hence of the luminosity along the RGB) is discernible. Giants in NGC 2808 show from moderate to large star-to-star abundance variations in Mg content, with an average value $[Mg/Fe]=0.26$ dex and a rms scatter of $\sigma = 0.16$ dex (31 stars). The Al abundance presents much larger variations, with a mean ratio $[Al/Fe]=+0.46$ dex and a higher rms scatter ($\sigma = 0.47$ dex). On the other hand, the sum $Al+Mg$ appears constant, with an average value $[(Mg+Al)/Fe]=+0.33$ and a very small dispersion ($\sigma = 0.05$ dex).

We recovered all stars with a sub-solar Mg abundance found in the previous studies, three from the NAO sample (Carretta et al. 2009b) and one from the SV sample (Paper I). All of them are actual detections, not upper limits. The combined sample brings to four the number of stars with subsolar Mg abundance in NGC 2808. Stars with such a low abundance are a notable exception among the GCs, apart from NGC 2419 (Mucciarelli et al. 2012; Cohen & Kirby 2012) and M 13 (Snedden et al. 2004). The relatively high frequency of stars with strong depletion in Mg, cou-

pled to the high temperature (~ 70 MK) required for the reactions of the Mg-Al cycle to occur, indicate that a fraction of stars in NGC 2808 was formed by matter extremely processed by hot H-burning.

Even more interestingly, the better statistics from the present homogeneous analysis clearly reveals that the RGB stars of the merged sample are not continuously distributed along the Mg-Al anticorrelation, but are instead clustered into three distinct groups (Fig. 3, upper panel). Using the distribution of stars along the Na-O anticorrelation in several GCs, Carretta et al. (2009a) divided the stellar population in each cluster in primordial (first generation) and intermediate and extreme components of second generation. By analogy, we associate the three groups along the Mg-Al anticorrelation in NGC 2808 with the same P, I, E components in order of increasing Al abundance (and decreasing Mg content). The groups include $68 \pm 15\%$, $19 \pm 8\%$, and $13 \pm 4\%$ of stars in our sample, respectively, where the associated uncertainties are Poisson errors. Within the quoted statistical uncertainties these fractions of stars derived from the Mg-Al anticorrelation are in excellent agreement with those estimated in Carretta et al. (2006) from the O-normal ($61 \pm 7\%$), O-poor ($22 \pm 4\%$) and super O-poor ($17 \pm 4\%$) RGB stars in NGC 2808 observed with GIRAFFE. A more accurate comparison must however await the re-analysis with the new, homogeneous temperature scale of all stars observed with both UVES and GIRAFFE.

No spurious effect due to the analysis can be responsible for the segregation of stars into these groups. Even corrections for departures from LTE can have only a negligible impact on this result, as shown in Fig. 2 (lower panel) where we plot the $[\text{Al}/\text{Mg}]$ ratios as a function of T_{eff} , indicating stars of different groups with different symbols. Giants with very similar atmospheric parameters, that would be equally affected by possible NLTE corrections and uncertainties in atmospheric parameters, are neatly segregated into the three P, I, E groups.

We show in the upper panel of Fig. 4 the distribution of the $[\text{Al}/\text{Mg}]$ ratios, that actually maximize the signal along the anticorrelation and allows us to nicely trace the three distinct clumps of stars separated by gaps at $[\text{Al}/\text{Mg}] \sim 0.5$ dex and $[\text{Al}/\text{Mg}] \sim 1.15$ dex. The three components are characterized by very different average values of the $[\text{Al}/\text{Mg}]$ ratio: -0.191 ± 0.035 dex ($\sigma = 0.160$ dex, 21 P stars), $+0.818 \pm 0.065$ dex ($\sigma = 0.158$ dex, 6 I stars), and $+1.310 \pm 0.050$ dex ($\sigma = 0.100$ dex, 4 E stars).

To evaluate how sound is this division, in the lower panel of Fig. 4 we plot the cumulative distribution of $[\text{Al}/\text{Mg}]$ ratios for each of the P,I,E group. A Kolmogorov-Smirnov test always allows to reject the null hypothesis that the three components are extracted from the same parent population, **with** $> 99.999\%$ **confidence**.

There is also a hint that the average metallicity slightly increases with the $[\text{Al}/\text{Mg}]$ ratio, from $[\text{Fe}/\text{H}] = -1.136$ dex ($\sigma = 0.032$ dex) for the P group to $[\text{Fe}/\text{H}] = -1.120$ dex ($\sigma = 0.020$ dex) and $[\text{Fe}/\text{H}] = -1.110$ dex ($\sigma = 0.006$ dex) for the I and E components, respectively. Although these values cannot be considered formally different with a high level of confidence, this finding is in qualitatively agreement with the prediction that more He-enrichment in more polluted stars (e.g. D’Antona et al. 2002) would

also increase the strength of metallic lines in stars with the same original metal abundance (Böhm-Vitense 1979), confirming the result obtained from a larger sample by Bragaglia et al. (2010) in NGC 2808.

4. DISCUSSION AND CONCLUSIONS

In the present study we were able to provide a chemical tagging of three distinct groups of stars along the Mg-Al anticorrelation on the RGB in NGC 2808, using the largest homogeneous set of Mg and Al abundances for giants in this cluster. The separation among the three groups on the RGB is much clearer in NGC 2808 than in NGC 6752 (Carretta et al. 2012; Milone et al. 2013). On the other hand, the three MSs in NGC 6752 seem to stand out less clearly than in the benchmark of multiple MSs represented by NGC 2808 (see Milone et al. 2012, 2013). This is not unexpected, because NGC 2808 is much more massive than NGC 6752 and it is currently well assessed that the cluster total mass is the main parameter driving the phenomenon of multiple populations in GCs (Carretta et al. 2010).

The fractions of stars in each of the P, I, and E components we found on the RGB are in very close agreement with the number ratios found for single MS stars in NGC 2808 by Milone et al. (2012): $62 \pm 2\%$, $24 \pm 2\%$, and $14 \pm 3\%$ for the red, middle and blue MS, respectively.

Having found three discrete populations of RGB stars, each characterized by a different chemical composition, we may ask what is the impact of this result on the formation scenario and the elusive nature of first generation polluters. Two commonly adopted scenarios (where the polluters are either rotating massive stars, Decressin et al. 2007 or intermediate-mass AGB stars, Ventura et al. 2001) share the need of dilution of the nucleically processed matter with unprocessed, pristine gas (Prantzos et al. 2007; D’Ercole et al. 2011). We then plot in the lower panel of Fig. 3 two simple dilution models, as in Carretta et al. (2009b). The first, adopting as polluted and original abundance ratios the extremes observed in NGC 2808, is able to reproduce the E and P groups: however, the I component is clearly left out. To be matched by this model, $[\text{Mg}/\text{Fe}]$ and $[\text{Al}/\text{Fe}]$ should be lowered, on average, by about 0.10 and 0.20 dex, respectively: the last value is about 4σ off the plausible range. On the other hand, if we arbitrarily change the starting values of Mg and Al to fit simultaneously the I and E components, the primordial level of Mg and Al would be inconsistent with what is actually observed. To summarize, there is no way to reproduce the intermediate component by mixing primordial and extremely polluted gas. As in the previous case of NGC 6752 we must conclude again that different polluters acted to produce the chemical composition observed in the I and E groups.

The strongly Mg-depleted stars observed in NGC 2808 represent a difficult problem for aforementioned formation scenarios. Discrete distribution of He values has been invoked as a likely way to explain both the three distinct MSs and the multimodal distribution of stars on the HB of NGC 2808 (D’Antona et al. 2005). The bluest MS is reproduced using a model with a helium mass fraction of $Y \sim 0.38$, and this should then be the He content of stars in the Mg-poor group, the E component. However, in one of the latest formulation of the AGB-based

formation scenario (D’Ercole et al. 2012) the largest Mg depletions are not from the super AGB, but come from AGB stars of $5\text{--}6M_{\odot}$. The He content of these stars is $Y \leq 0.34$ (see Tab. 1 in D’Ercole et al. 2012), which is the threshold above which the authors adopt a deep-mixing scheme able to decrease the O abundance in second generation He-rich stars down to the very low values $[\text{O}/\text{Fe}] \sim -0.8 \div -1.0$ observed in GCs like NGC 2808 (Paper I) or M 13 (Johnson & Pilachowski 2012). Unfortunately, the very Mg-poor stars of the E component are also the most O-poor stars in NGC 2808 (Carretta et al., in preparation). Hence, as advanced by D’Ercole et al. (2012), this extreme population constitutes a problem for any pollution model and for the deep mixing scenario. On the other hand, efficient destruction of Mg and enhancement of Al are apparently produced by FRMS only at the end of the MS, but with simultaneous strong Na destruction (Decressin et al. 2007), which is again not well matched by observations.

In summary:

1) we put on a better statistical base the known Mg-Al anticorrelation observed in NGC 2808 (Carretta et al. 2009b), more than doubling the size of the sample of stars with homogeneous Mg and Al abundances. The anticorrelation is very extended, reaching a regime where very Mg-poor giants are found, a rare occurrence among GC stars.

2) for the first time we found clear evidence of three discrete populations each with distinctly homogeneous chemical composition on the RGB of NGC 2808. The first group P has the primordial composition of field stars of similar metallicity, and the I and E components show signatures of increasing processing of matter in hot H-burning.

3) the fractions of P,I,E stars along the Mg-Al anticorrelation are in excellent agreement with the number ratios found by Milone et al. (2012) for the three MSs in NGC 2808. We conclude that P, I, and E stars represent the progeny of the red, intermediate and blue main sequences, with increasing He content.

4) No simple dilution model appears to be able to simultaneously reproduce the chemistry of the three discrete components in NGC 2808, suggesting again that in this cluster two different classes of first generation polluters were at work. This is also seen in NGC 6752, another GCs with three discrete stellar populations spectroscopically detected on the RGB.

Future steps include enlarging the set of Al abundances in this GC: a program to measure the $[\text{Al}/\text{Fe}]$ ratios of more than 100 giants in NGC 2808 using the HR21 setup of GIRAFFE and the strong Al doublet at $8772\text{--}74\text{ \AA}$ was just granted observing time at the ESO@VLT. Moreover, the homogeneous reanalysis of other elements, in particular the proton-capture species O, Na, Si, with the proper temperature scale, is in progress, to provide the full network of correlations and anticorrelations in this peculiar globular cluster.

We thank Angela Bragaglia and Michele Bellazzini for valuable help and suggestions. This publication makes use of data products from the Two Micron All Sky Survey, which is a joint project of the University of Massachusetts and the Infrared Processing and Analysis Cen-

ter/California Institute of Technology, funded by the National Aeronautics and Space Administration and the National Science Foundation. This research has been funded by PRIN INAF 2011 "Multiple populations in globular clusters: their role in the Galaxy assembly" (PI E. Carretta), and PRIN MIUR 2010-2011, project "The Chemical and Dynamical Evolution of the Milky Way and Local Group Galaxies" (PI F. Matteucci).

REFERENCES

- Alonso, A., Arribas, S. & Martinez-Roger, C. 1999, *A&AS*, 140, 261
 Alonso, A., Arribas, S. & Martinez-Roger, C. 2001, *A&A*, 376, 1039
 Bedin, L.R., Piotto, G., Zoccali, M., Stetson, P.B., Saviane, I., Cassisi, S., & Bono, G. 2000, *A&A*, 363, 159
 Böhm-Vitense, E. 1979, *ApJ*, 234, 521
 Bragaglia, A., Carretta, E., Gratton, R.G., D’Orazi, V., Cassisi, S., Lucatello, S. 2010, *A&A*, 519, 60
 Carretta, E., Bragaglia, A. & Cacciari 2004a, *ApJ*, 610, L25
 Carretta, E., Gratton R.G., Bragaglia, A., Bonifacio, P., Pasquini, L. 2004b, *A&A*, 416, 925
 Carretta, E. 2006, *AJ*, 131, 1766 (Paper I)
 Carretta, E., Bragaglia, A., Gratton R.G., Leone, F., Recio-Blanco, A., Lucatello, S. 2006, *A&A*, 450, 523
 Carretta, E., Recio-Blanco, A., Gratton, R.G., Piotto, G., Bragaglia, A. 2007a, *ApJ*, 671, L125
 Carretta, E., Bragaglia, A., Gratton, R.G., Lucatello, S. Momany, Y. 2007b, *A&A*, 464, 927
 Carretta, E., Bragaglia, A., Gratton, R.G. et al. 2009a, *A&A*, 505, 117
 Carretta, E., Bragaglia, A., Gratton, R.G., Lucatello, S. 2009b, *A&A*, 505, 139
 Carretta, E., Bragaglia, A., Gratton, R.G., Recio-Blanco, A., Lucatello, S., D’Orazi, V., Cassisi, S. 2010, *A&A*, 516, 55
 Carretta, E., Bragaglia, A., Gratton, R.G., D’Orazi, V., Lucatello, S. 2011, *A&A*, 535, 121
 Carretta, E., Bragaglia, A., Gratton, R.G., Lucatello, S., D’Orazi, V. 2012, *ApJ*, 750, L14
 Carretta, E., Bragaglia, A., Gratton, R.G., et al. 2014, *A&A*, 564, A60
 Cohen, J.G., Kirby, E.N. 2012, *ApJ*, 760, 86
 Cordero, M.J., Pilachowski, C.A., Johnson C.I., McDonald, I., Zijlstra, A.A., Simmerer, J. 2014, *ApJ*, 780, 94
 D’Antona, F., Caloi, V., Montalbán, J., Ventura, P., Gratton, R. 2002, *A&A*, 395, 69
 D’Antona, F., Bellazzini, M., Caloi, V., Fusi Pecci, F., Galletti, S., Rood, R.T. 2005, *ApJ*, 631, 868
 Decressin, T., Meynet, G., Charbonnel C. Prantzos, N., Ekstrom, S. 2007, *A&A*, 464, 1029
 Denisenkov, P.A., Denisenkova, S.N. 1989, *A&AS*, 1538, 11
 D’Ercole, A., D’Antona, F., Vesperini, E. 2011, *MNRAS*, 415, 1304
 D’Ercole, A., D’Antona, F., Carini, R., Vesperini, E., Ventura, P. 2012, *MNRAS*, 423, 1521
 Gratton, R.G. 1988, *Rome Obs. Preprint Ser.*, 29
 Gratton, R.G. et al. 2001, *A&A*, 369, 87
 Gratton, R.G., Carretta, E., Claudi, R., Lucatello, S., & Barbieri, M. 2003, *A&A*, 404, 187
 Gratton, R.G., Carretta, E., Bragaglia, A., & Lucatello, S., D’Orazi, V. 2010, *A&A*, 517, 81
 Gratton, R.G., Lucatello, S., Carretta, E., Bragaglia, A., D’Orazi, V., Momany, Y. 2011, *A&A*, 534, 123
 Gratton, R.G., Carretta, E., Bragaglia, A. 2012, *A&ARv*, 20, 50
 Harris, W.E. 1996, *AJ*, 112, 1487
 Johnson, C.I., Pilachowski, C.A. 2012, *ApJ*, 754, L38
 Kraft, R. P. 1994, *PASP*, 106, 553
 Kurucz, R.L. 1993, *CD-ROM 13*, Smithsonian Astrophysical Observatory, Cambridge
 Langer, G.E., Hoffman, R., & Sneden, C. 1993, *PASP*, 105, 301
 Magain, P. 1984, *A&A*, 134, 189
 Marino, A.F., Villanova, S., Piotto, G., Milone, A.P., Momany, Y., Bedin, L.R., Medling, A.M. 2008, *A&A*, 490, 625

- Milone, A.P., Bedin, L., Piotto, G. et al. 2008, *ApJ*, 673, 241
- Milone, A.P., Piotto, G., Bedin, L., Cassisi, S., Anderson, J., Marino, A.F., Pietrinferni, A., Aparicio, A. 2012, *A&A*, 537, A77
- Milone, A.P., Marino, A.F., Piotto, G. et al. 2013, *ApJ*, 767, 120
- Mucciarelli, A., Bellazzini, M., Ibata, R., Merle, T., Chapman, S.C., Dalessandro, E., Sollima, A. 2012, *MNRAS*, 426, 2889
- Piotto, G., Bedin, L., Anderson, J. et al. 2007, *ApJ*, 661, L53
- Prantzos, N., Charbonnel, C., Iliadis, C. 2007, *A&A*, 470, 179
- Skrutskie, M.F. et al. 2006, *AJ*, 131, 1163
- Snedden, C., Kraft, R.P., Guhathakurta, P., Peterson, R.C., Fulbright, J.P. 2004, *AJ*, 127, 2162
- Ventura, P. D'Antona, F., Mazzitelli, I., & Gratton, R. 2001, *ApJ*, 550, L65
- Yong, D., Grundahl, F., Nissen, P.E., Jensen, H.R., Lambert, D.L. 2005, *A&A*, 438, 875

Table 1
Magnitudes, atmospheric parameters, [Mg/Fe], and [Al/Fe] ratios for red giants in NGC 2808.

star	RA,DEC	<i>B</i>	<i>V</i>	<i>K</i>	<i>T</i> _{eff}	log <i>g</i>	[A/H]	<i>v</i> _t	nr [Mg/Fe] σ	nr [Al/Fe] σ
8739	9 11 51.20 -64 48 37.54	15.761	14.288	10.693	4271	1.13	-1.12	1.63	3 +0.325 0.122	2 +0.027 0.061
38660	9 12 39.87 -64 55 43.08	15.672	14.290	10.875	4318	1.21	-1.13	1.67	3 +0.361 0.070	2 +0.070 0.007
8603	9 12 14.05 -64 48 42.92	15.847	14.432	10.957	4339	1.24	-1.14	1.61	3 +0.319 0.088	2 +0.030 0.024
10571	9 12 41.12 -64 46 25.85	15.806	14.376	10.844	4310	1.19	-1.13	1.56	3 +0.342 0.115	2 +0.152 0.057
30763	9 11 31.62 -64 54 57.99	15.927	14.606	11.465	4469	1.48	-1.11	1.63	2 -0.078 0.020	2 +1.232 0.045
49743	9 12 36.80 -64 51 45.10	16.353	15.168	12.159	4647	1.77	-1.10	1.59	2 -0.072 0.045	2 +1.171 0.084
34008	9 11 27.52 -64 51 31.29	16.346	15.119	12.115	4636	1.75	-1.11	1.56	2 -0.104 0.022	2 +1.132 0.088
38228	9 12 30.97 -64 56 8.52	16.211	14.981	11.887	4577	1.65	-1.10	1.66	3 +0.358 0.022	2 +0.242 0.018
10105	9 12 21.15 -64 47 13.91	15.976	14.669	11.417	4457	1.45	-1.16	1.42	3 +0.297 0.104	2 -0.039 0.035
7536	9 12 31.71 -64 49 22.27	15.812	14.372	10.829	4306	1.18	-1.11	1.55	3 +0.355 0.095	2 +0.201 0.007
44984	9 12 45.88 -64 53 1.41	15.855	14.535	11.219	4406	1.36	-1.13	1.59	3 +0.335 0.066	2 +0.032 0.033
33918	9 11 1.69 -64 51 36.09	15.776	14.331	10.887	4321	1.22	-1.11	1.63	3 +0.357 0.088	2 +0.352 0.042
48889	9 12 8.51 -64 51 58.47	15.139	13.341	9.253	3902	0.52	-1.14	1.91	3 +0.161 0.060	2 +1.003 0.091
51983	9 12 2.50 -64 51 10.07	15.328	13.474	9.182	3884	0.48	-1.15	1.86	3 +0.247 0.080	2 +1.024 0.101
47606	9 12 6.66 -64 52 18.23	15.257	13.436	9.103	3864	0.44	-1.12	1.72	3 +0.440 0.052	2 +0.131 0.051
51499	9 12 7.35 -64 51 17.80	15.157	13.435	9.382	3935	0.57	-1.21	1.83	3 +0.342 0.052	2 +0.055 0.049
46580	9 11 56.19 -64 52 35.39	15.292	13.690	9.790	4040	0.78	-1.13	1.81	3 +0.268 0.045	2 +0.321 0.008
48609	9 12 16.64 -64 52 2.92	15.285	13.415	9.101	3863	0.44	-1.14	1.84	3 +0.415 0.083	2 +0.041 0.047
50761	9 11 57.08 -64 51 29.68	15.394	13.390	9.224	3895	0.31	-1.17	1.65	3 +0.334 0.051	2 +0.512 0.006
37872	9 12 23.07 -64 56 34.30	15.334	13.650	9.711	4020	0.71	-1.10	1.84	3 +0.218 0.070	2 +1.150 0.045
51454	9 12 2.28 -64 51 18.51	15.233	13.446	9.244	3900	0.51	-1.18	1.78	3 +0.398 0.082	2 +0.083 0.023
50119	9 11 42.92 -64 51 39.75	15.425	13.886	10.218	4150	0.93	-1.11	1.80	2 -0.115 0.033	2 +1.336 0.035
46422	9 11 56.09 -64 52 37.90	15.174	13.376	9.197	3888	0.44	-1.18	1.93	3 +0.385 0.067	2 +0.078 0.007
46099	9 12 33.58 -64 52 43.09	15.375	13.741	9.835	4052	0.76	-1.15	1.85	3 +0.348 0.075	2 +0.235 0.006
53390	9 11 52.95 -64 50 47.86	15.958	14.669	11.379	4447	1.43	-1.12	1.49	3 +0.349 0.045	1 +0.018 9.999
43217	9 12 32.67 -64 53 32.87	17.471	16.440	13.675	5036	2.41	-1.11	1.59	1 +0.272 9.999	2 +0.360 0.011
13983	9 11 39.79 -64 48 25.46	17.027	15.940	13.092	4886	2.16	-1.11	1.10	2 +0.126 0.078	2 +1.156 0.011
10201	9 12 45.76 -64 47 5.39	16.864	15.714	12.759	4801	2.02	-1.11	1.43	2 +0.231 0.037	2 +0.986 0.021
42886	9 12 59.11 -64 53 38.61	17.019	15.921	13.040	4873	2.14	-1.14	0.64	1 +0.284 9.999	1 +0.230 9.999
32685	9 11 27.07 -64 52 44.38	16.794	15.656	12.772	4804	2.03	-1.11	0.61	2 +0.292 0.025	2 +0.863 0.006
56032	9 11 45.58 -64 50 4.21	15.579	13.976	10.095	4118	0.87	-1.07	1.78	3 +0.364 0.056	2 +0.111 0.002

^a Identification, coordinates, and *B*, *V* magnitudes from Bedin et al. (2000)

^b *K* magnitudes from Skrutskie et al. (2006)

^c Atmospheric parameters from Carretta et al. (in preparation).

^d σ is the *rms* scatter of the mean.

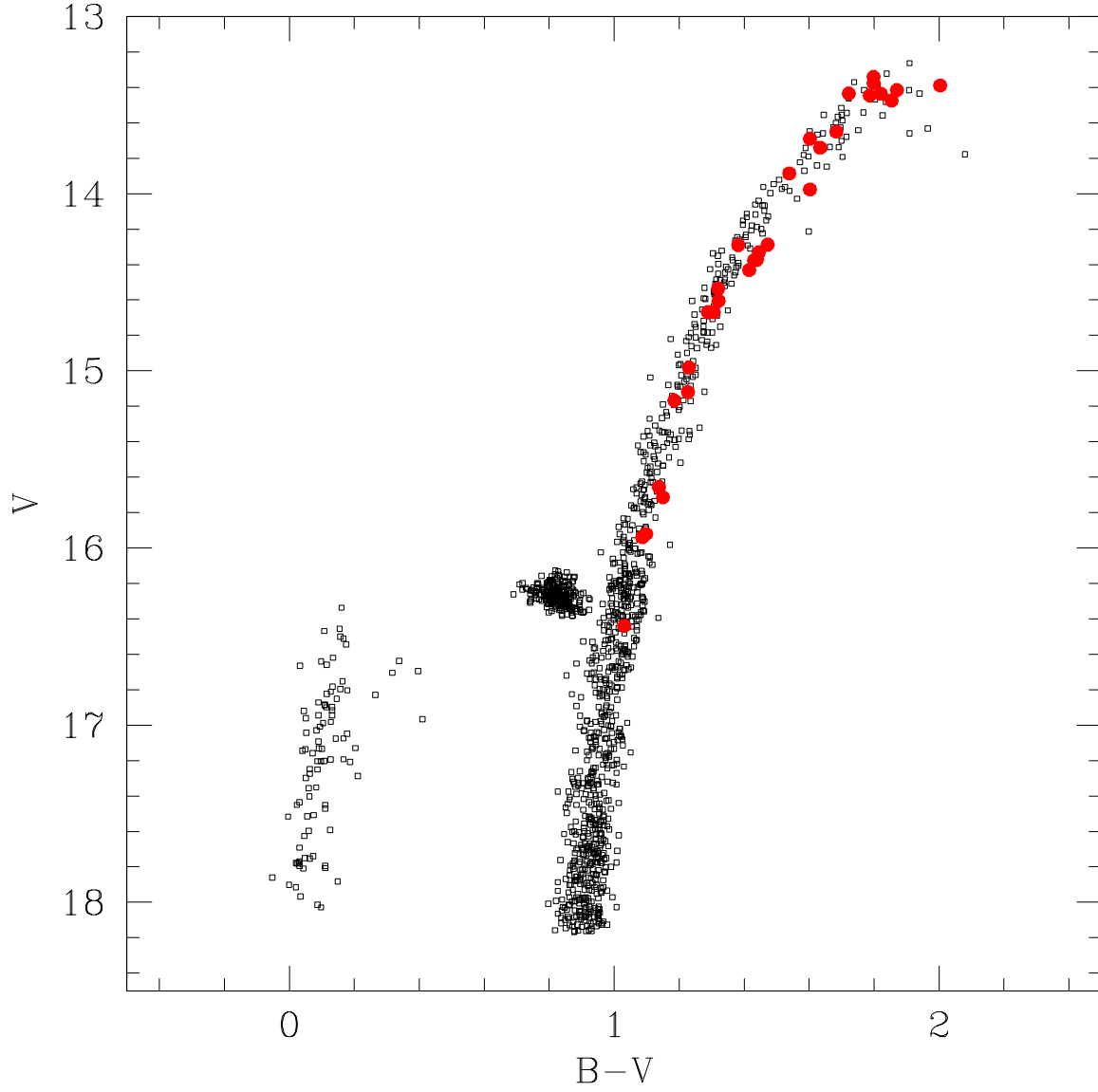


Figure 1. $(V, B - V)$ color-magnitude diagram of NGC 2808 from Bedin et al. (2000). Stars in the present study are marked with large filled circles.

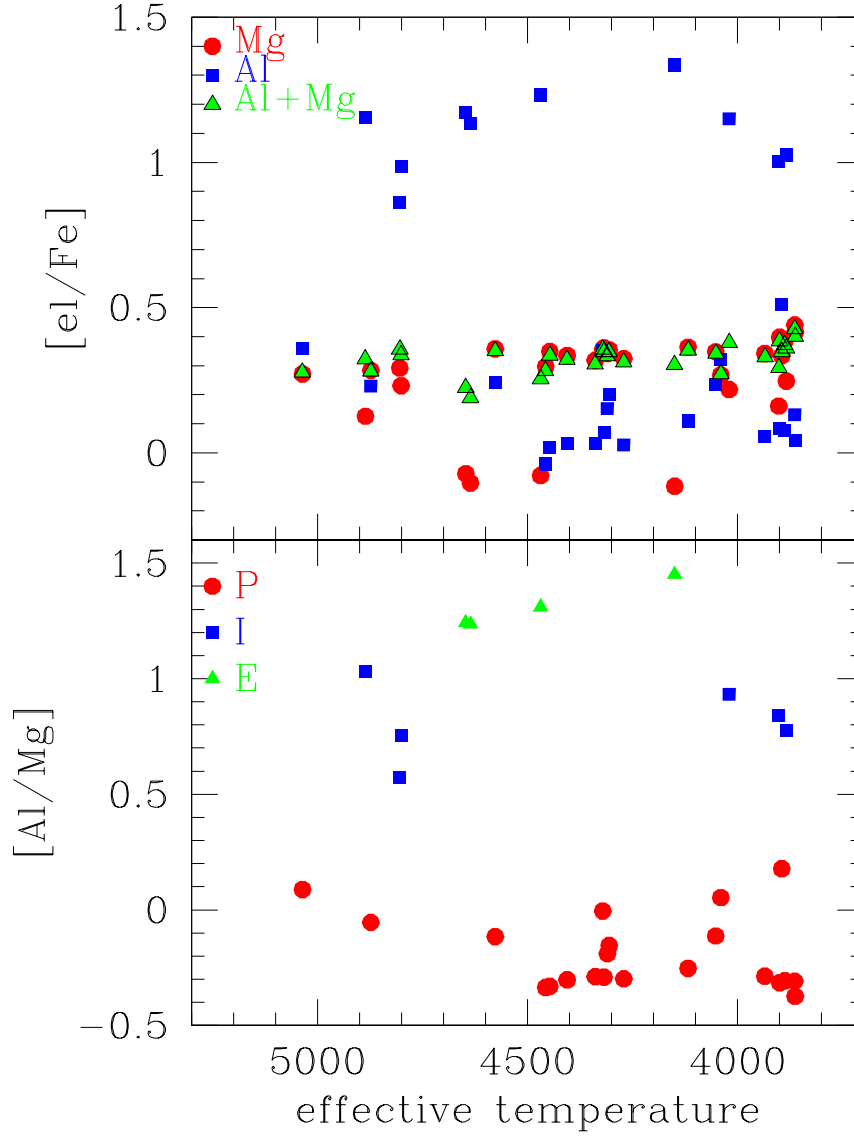


Figure 2. Upper panel: $[\text{Mg}/\text{Fe}]$ (circles), $[\text{Al}/\text{Fe}]$ (squares), and $[(\text{Al}+\text{Mg})/\text{Fe}]$ (triangles) abundance ratios as a function of the effective temperature. Lower panel: $[\text{Al}/\text{Mg}]$ ratios as a function of the temperature. Different symbols indicate stars of the three groups (see text and Fig. 3).

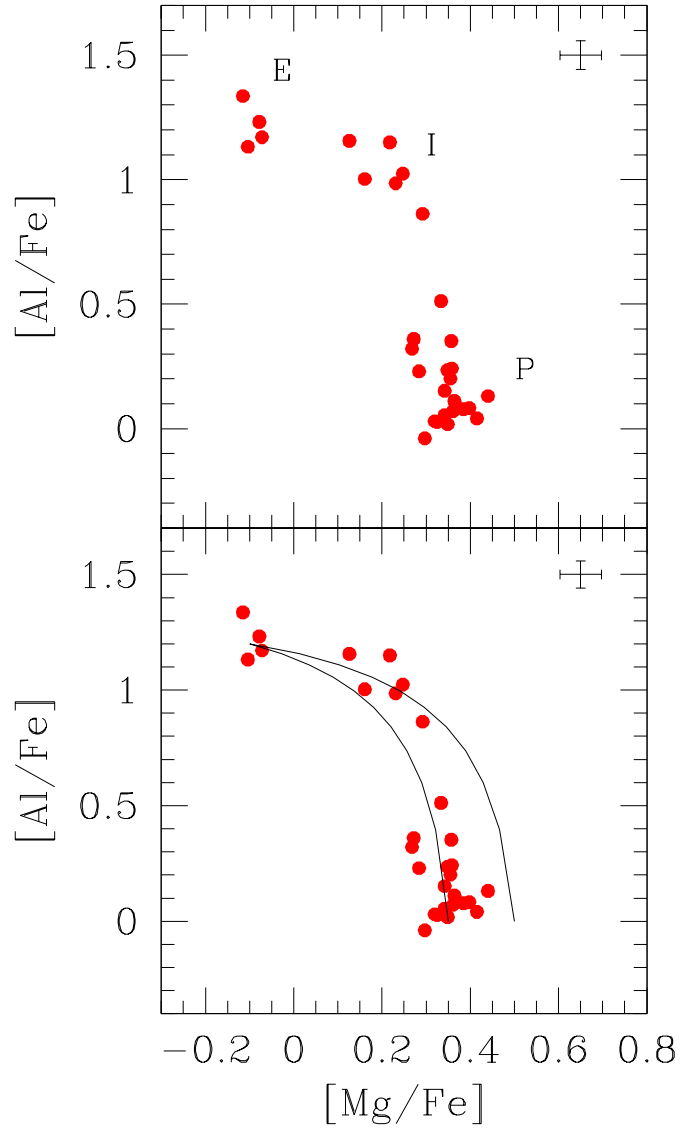


Figure 3. Upper panel: Mg-Al anticorrelation in NGC 2808. Star to star error bars are indicated. Lower panel: the same plot, with two dilution models superimposed, starting at different primordial Mg levels.

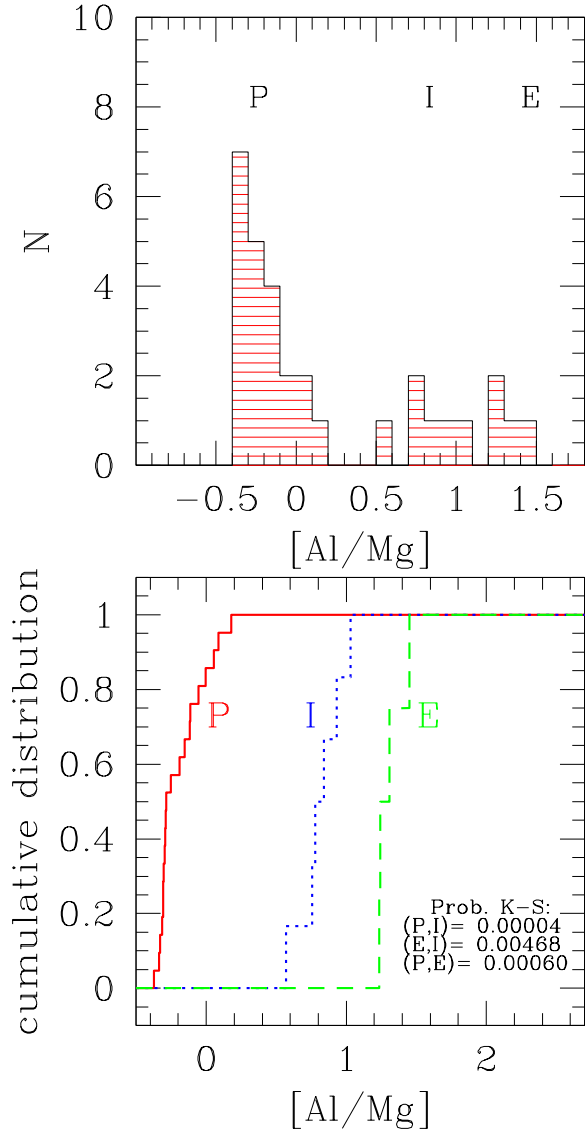


Figure 4. Upper panel: distribution of $[\text{Al}/\text{Mg}]$ ratios for the entire sample of giants in NGC 2808. Lower panel: cumulative distributions of $[\text{Al}/\text{Mg}]$ ratios in the P (solid line), I (dotted line), and E (dashed line) groups. The probabilities of the Kolmogorov-Smirnov test are also indicated.